1. Walid Mohammed KACEMI[1], 2. Elhadj BOUNADJA[2],3. Abdelkadir BELHADJ DJILALI[3],4. Belkacem SELMA[4]

[1,2,3,4]Laboratoire de génie électrique et énergies renouvelables (LGEER), Hassiba Benbouali University of Chlef, B.P 78C, Ouled Fares, Chlef, 02180, Algeria.

ORCID: 1.0000-0002-3528-3026; 2.0000-0002-3002-4316;3.0000-0001-6015-5731;4.0000-0002-8678-5739

doi:10.15199/48.2024.04.08

Enhancing Wind Energy Conversion Efficiency with Parallel Hybrid Excitation Synchronous Generators based on Second-Order Sliding Mode Control

Abstract. *The increasing popularity of Hybrid Excitation Synchronous Generators (HESGs) has drawn significant attention from researchers and industrialists due to their simple and sturdy structure, as well as their high-speed operation. These generators find widespread utilization in various applications, with a particular focus on renewable energy, especially in the context of wind energy conversion systems (WECS). The research presents a novel variable structure control method for a WECS that incorporates two three-phase hybrid excitation synchronous generators connected to a diode bridge rectifier. The system can function as a DC generator for isolated loads in embedded applications. The traditional control techniques, such as integral-proportional (PI) controllers, have shown drawbacks in terms of power quality and performance in WECS. To address these issues, the study proposes a new strategy based on second-order sliding mode (SOSM) control. This technique is used for the purpose of improving control performance in WECS. The primary goal of the SOSM control is to maintain a steady DC bus voltage even when the DC load and rotor speed vary. The simulation and modeling of the entire system are carried out using MATLAB/ Simulink. The results demonstrate the efficacy of the proposed conversion method, proving its effectiveness in power generation applications.*

Streszczenie. *Rosnąca popularność synchronicznych generatorów hybrydowego wzbudzenia (HESG) przyciągnęła znaczną uwagę naukowców i przemysłowców ze względu na ich prostą i solidną konstrukcję, a także ich szybkie działanie. Generatory te znajdują szerokie zastosowanie w różnych zastosowaniach, ze szczególnym uwzględnieniem energii odnawialnej, zwłaszcza w kontekście systemów konwersji energii wiatrowej (WECS). Badania przedstawiają nowatorską metodę sterowania zmienną strukturą WECS, która obejmuje dwa trójfazowe hybrydowe generatory synchroniczne ze wzbudzeniem połączone z diodowym mostkiem prostowniczym. System może działać jako generator prądu stałego dla izolowanych obciążeń w aplikacjach wbudowanych. Tradycyjne techniki sterowania, takie jak regulatory całkowo-proporcjonalne (PI), wykazały wady pod względem jakości energii i wydajności w WECS. Aby rozwiązać te problemy, w badaniu zaproponowano nową strategię opartą na sterowaniu w trybie ślizgowym drugiego rzędu (SOSM). Ta technika jest używana w celu poprawy wydajności kontroli w WECS. Głównym celem sterowania SOSM jest utrzymanie stałego napięcia szyny DC, nawet gdy zmienia się obciążenie DC i prędkość wirnika. Symulacja i modelowanie całego systemu odbywa się za pomocą MATLAB/Simulink. Wyniki pokazują skuteczność proponowanej metody konwersji, udowadniając jej skuteczność w zastosowaniach związanych z wytwarzaniem energii. (**Zwiększanie efektywności konwersji energii wiatrowej za pomocą równoległych generatorów synchronicznych o wzbudzeniu hybrydowym opartych na sterowaniu trybem ślizgowym drugiego rzędu**)*

Keywords: Hybrid Excitation Synchronous Generator (HESG), Diode bridge rectifier, DC bus voltage, Second-order sliding mode controller (SOSMC). Wind Power Generation System (WPGS).
Słowa kluczowe: Hybrydowy generator synchroniczny z wzbudzeniem (HESG), diodowy mostek prostowniczy, napięcie szyny DC, kontroler trybu ślizgowego drugiego rzędu (SOSMC). System wytwarzania energii wiatrowej (WPGS).

Introduction

Due to significant industrial expansion and population growth, the global demand for electrical energy has grown dramatically in recent decades. Thus, traditional fossil fuel consumption has escalated, causing global warming, pollution, and fossil energy depletion. Solar, wind, and hydropower are needed to solve these issues [1], [2]. Wind power is one of the fastest-growing renewable energy sources [3], [4]. Wind energy interest increased global installed wind energy capacity to 743 GW by 2020, with 93 GW of wind power capacity [5].

Variable-speed wind power conversion systems (WPCS) convert wind energy into electricity. They reduce mechanical stress, reactive power, voltage fluctuation, and energy absorption at various rotation speeds [6]. DFIG and PMSG systems convert variable-speed wind energy into electricity. DFIG is the best WPCS because it can work at different speeds, control active and reactive power individually, collect the most mechanical power, and cost less. Power electronic converters are 30% as powerful as the generator [7]. However, DFIG needs frequent maintenance, slide rings and brushes lose electricity, and grid disruptions can damage it [8]. The PMSG with a full-power converter is more efficient, reliable, self-exciting, and low-maintenance [9].

Wind power conversion systems (WPCS) have recently proposed new generator kinds. The hybrid excitation synchronous generator (HESG) is a variable-speed system that ensures a consistent frequency output in WPCS and hydroelectric power facilities with fluctuating heads [10,11,12]. The HESG improves steady-state and dynamic stability [13] and system reliability [14,15].

This study proposes using two three-phase hybrid excitation synchronous generators coupled to a diode bridge rectifier to improve wind energy conversion system performance. The technology generates DC power for embedded loads. In WPCS, integral-proportional (PI) controllers limit power quality and performance. The paper introduces second-order sliding mode (SOSM) variable structure control to overcome these issues. This methodology improves WPCS traditional control methods by maintaining a stable DC bus voltage regardless of DC load and rotor speed. These simulations show that the SOSM control technique can optimise wind energy conversion systems. Fig. 1 shows the conversion system configuration.

The following is how this paper is organized: Section 2 describes the modelling of the HESG-based WPGS, including HESG classification, wind turbine modelling with its MPPT, and HESG modelling. Section 3 focuses on controlling two of HESG principles and introduces the proposed SOSMC for the WPGS-integrated two of HESG. Section 4 runs numerical simulations of the entire system depicted in Fig. 1 to validate the effectiveness and evaluate the performance of the pro-posed control. Finally, Section 5 contains the paper's conclusion and perspective.

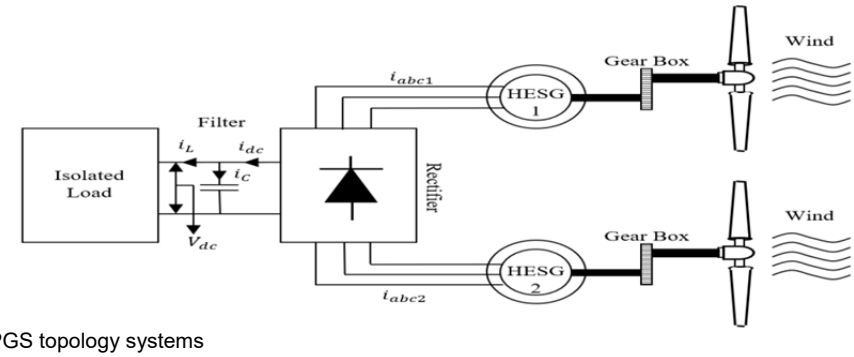

Fig.1. HESG-based WPGS topology systems

Description of system

Model of HESG

The physical description serves as the foundation for the initial modelling of the HESG. This explanation focused on the stator coil inductor [16,17]. The latter behaves similarly to the magnets if it is put on the rotor. As a result, a symbolic bipolar diagram of the HESG of the type shown in Fig. 2 can be proposed. On the latter, we see a fictitious rotor winding that is typical of the excitation stator winding [18].

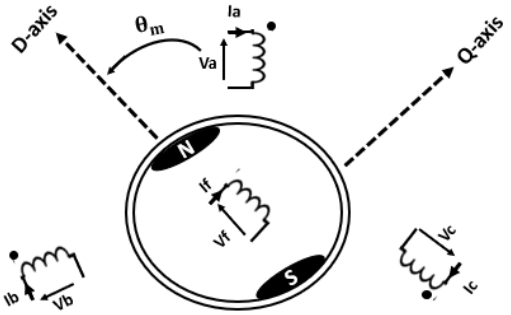

Fig.2. HESG windings representation.

• The fluxes of the three stator phases are stated as follows:

$$[\psi_s] = [L_s][i_s] + [\psi_{pm}] + [L_{sf}].i_f \quad (1)$$

Where: $[L_s]$: Matrix of stator-stator coupling inductors; $[\psi_{pm}]$: Flux of the magnets defined by (2); $[L_{sf}]$: Stator–rotor coupling matrix.

$$[\psi_{pm}] = \psi_a \begin{bmatrix} cos(\theta) \\ cos\left(\theta - \frac{2\pi}{3}\right) \\ cos\left(\theta + \frac{2\pi}{3}\right) \end{bmatrix} \quad (2)$$

• The stator voltage equations take the following form:

$$[v_s] = [R_s][i_s] + \frac{d}{dt}[\psi_s] \quad (3)$$

With:

$[v_s] = [v_a \quad v_b \quad v_c]^T$: Stator voltage vector.

$[i_s] = [i_a \quad i_b \quad i_c]^T$: Vector of the stator currents.

• The rotor voltage is given by:

$$v_f = R_f.i_f + \frac{d\psi_f}{dt} \quad (4)$$

With: v_f : Rotor excitation voltage; i_f: Rotor excitation current; R_f: Rotor resistance; ψ_f: Rotor flux.

• The dynamic model of the HESG in the dq frame [18]

$$\begin{cases} \frac{di_\mu}{dt} = \frac{1}{L_d}\left(V_d - R_s i_\mu + mR_s i_f + p\Omega\left(L_q i_q - \psi_{pm}\right)\right) \\ \frac{di_q}{dt} = \frac{1}{L_q}\left(V_q - R_s i_q - p\Omega\left(L_d i_\mu\right)\right) \\ \frac{di_f}{dt} = \frac{1}{\sigma L_f}\left(V_f - R_f i_f - m e_\mu\right) \\ \frac{d\Omega}{dt} = \frac{1}{J}(C_{em} - C_r - f_v\Omega) \end{cases} \quad (5)$$

Model of Turbine

Equation (6) defines the theoretical power output of a turbine using air density, rotor circumference, blade pitch, and wind velocity [19].

$$P_t = C_p P_v = \frac{1}{2}\rho\pi R^2 v^3 C_p(\lambda, \beta) \quad (6)$$

Equation (7), where Ω_t represents the turbine's speed and R represents the blades' radius, illustrates the relationship between wind speed and turbine speed.

$$\lambda = \frac{R.\Omega_t}{v} \quad (7)$$

The "Betz limit," also known as the theoretical maximum for the power coefficient (Cp), is 0.475. However, this value is impractical. Utilize eq (8) to determine the value of this coefficient.

$$C_p(\lambda, \beta) = 0.5\left(\frac{116}{\lambda_i} - 0.4\beta - 5\right) exp\left(\frac{-21}{\lambda_i}\right) + 0.0068\lambda \quad (8)$$

This equation refers to the mechanical dynamics of the system on the mechanical shaft of the generator.

$$J\frac{d\Omega_g}{dt} = C_{méc} = C_g - C_{em} - C_f \quad (9)$$

From equation (6) to equation (9), a functional block diagram model and Maximum Power Point Tracking (MPPT) control of the turbine is established Fig. 3

The Converters models

The chopper-style DC-DC converter can be modelled using Equation (10), which can be found below. In direct current circuits, static chopper converters are widely employed to regulate the flow of energy between a source and a load to better manage the flow of electric power [20].

$$\begin{pmatrix} I_L \\ V_c \end{pmatrix} = \begin{pmatrix} 0 & -\frac{1}{L} \\ \frac{1}{C} & -\frac{1}{RC} \end{pmatrix}\begin{pmatrix} I_L \\ V_c \end{pmatrix} + \begin{pmatrix} 0 & \frac{1}{L} \\ -\frac{1}{C} & 0 \end{pmatrix}\begin{pmatrix} I_L \\ V_c \end{pmatrix} u + \begin{pmatrix} \frac{E}{L} \\ 0 \end{pmatrix} \quad (10)$$

The rectifier model is shown in equation (14) [21].

$$C\frac{dV_{dc}}{dt} = f_a.i_{as} + f_b.i_{bs} + f_c.i_{cs} - i_{ch} \quad (11)$$

In order to establish control, we make use of the technique shown in Fig. 4.

.

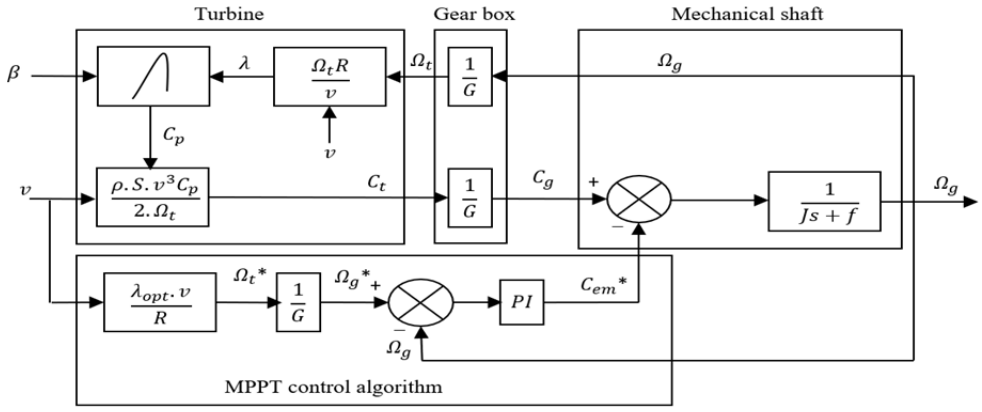

Fig 3: Wind turbine model with speed control block diagram.

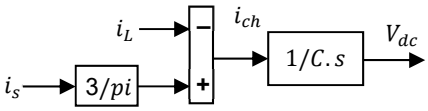

Fig 4: Control of a rectifier.

The voltage of the DC closed loop is represented in Fig. 5.

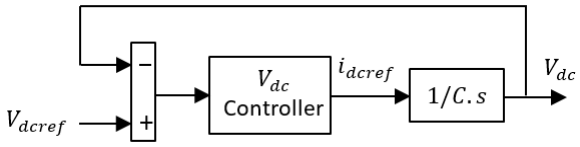

Fig 5: DC bus voltage closed loop.

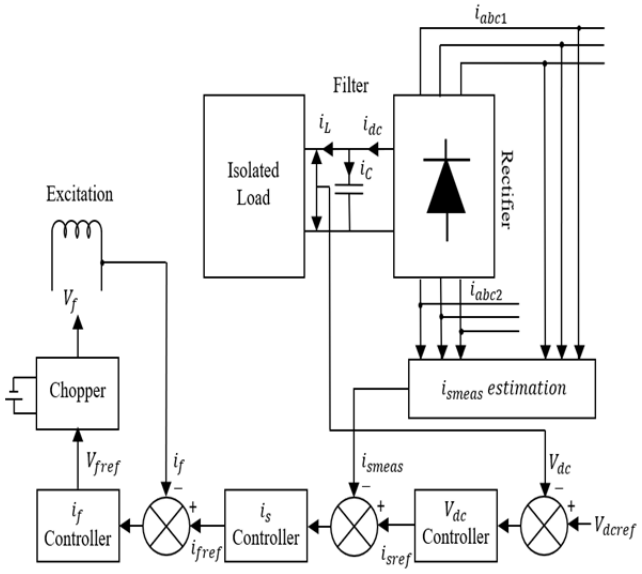

Fig 6: HESG-based WPCS control.

SOSMC Control

The objective of this instruction is to control the HESG's output voltage, Vdc. As a result, a rectifier is needed between the machine and the DC bus [21]. A diode bridge rectifier is suitable for this application because of its great dependability and low cost. The key advantage of adopting HESG is its high performance and the ability to be coupled with a diode rectifier [22], which decreases power electronics costs and losses [23,24]. In terms of structural complexity, this solution offers an undeniable benefit [25].

Let us begin by the principle of control. First, regulate the excitation coil current. This current regulates the flow of excitation, including permanent magnets and coiled excitation. We regulate the stator vacuum electromotive forces. After controlling stator currents, a three-phase source of current assaults the diode rectifier. Reversed voltage is dependent on reversed current. The structure and control of the conversion system are depicted in Fig 6.

For the Speed

The speed error can be described in terms of sliding surfaces [26]. In other words, we can represent it using the following expression:

(12) $$S_\Omega = \Omega_g{}^* - \Omega_g$$

The Second-order sliding mode control law comprises two parts. The first part, u_1, is a continuous function that depends on the sliding variable [27], while the second part, u_2, is defined by its time derivative [28]. The main objective of this proposed control strategy is to drive the sliding variable (S) to converge to zero, achieving $S = \dot{S} = 0$ in finite-time.

The proposed SOSMC controller can be mathematically represented as follows [29]:

(13) $$u = -u_1 - u_2$$

For the Speed:

Where:

(14) $$u_1 = \alpha . |S|^{\frac{1}{2}} . sign(S)$$

(15) $$\dot{u_2} = \beta . sign(S)$$

The speed control is achieved using the SOSMC to regulate the speed and can be expressed as follows:

(16) $$u_\Omega = -\alpha . |S_\Omega|^{\frac{1}{2}} . sign(S_\Omega) - \beta . sign(S_\Omega)$$

For the Stator Currents and DC bus Voltage

Stator current control cannot be accomplished with a resonant regulator because the chopper's input must be in direct current to control the current in the exciter winding. A regulator controls the amplitude of the stator current via the excitation current. Figure 8 shows how the outer loop of the output voltage calculates its reference.

The sliding surfaces for the currents and the DC bus voltage can be mathematically expressed as follows [30]:

(17) $$\begin{cases} S_{i_s} = {i_s}^* - i_s \\ S_{i_f} = {i_f}^* - i_f \end{cases}$$

(18) $$S_{V_{dc}} = V_{dc}^{*} - V_{dc}$$

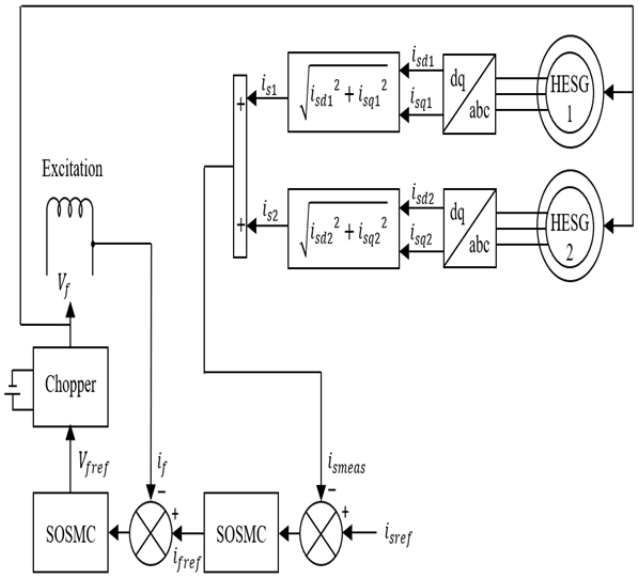

Fig 8: Excitation current control loop

Results & discussions

The examined control method (SOSMC), utilised in the context of the HESG-based WPCS control, as described in Section 3, was simulated using MATLAB software. Then, the performance metrics were evaluated and compared to those obtained with standard PI control, revealing critical insights into the system's effectiveness and dependability.

Table 3 in the appendix provides a comprehensive listing of the HESG-WPGS parameters.

In this study, simulations were conducted and analysed: with R = 10. In all simulation experiments conducted with the MATLAB software. The performance of both SOSMC and PI in the case of the wind speed illustrated in Fig. 9.

Figure 9 depicts the wind speed profiles of two wind turbines, with minimal and maximum values of 1.25 m/s and 16 m/s, respectively, and an average of 8.5 m/s. Figure 10 depicts the aerodynamic power generated by two wind turbines, with the first turbine reaching 10 kW when the wind speed increased to 14.75 m/s. In contrast, the second turbine's output reached 12 kW when the wind speed reached 16 m/s. The aerodynamic power of the system is the sum of the individual powers of turbines 1 and 2. Figure 11 depicts the curves that demonstrate the satisfactory performance of the proposed control strategies, SOSMC and PI control, with measured velocities closely aligning with the references. The diagram demonstrates the interaction and modulation of these distinct control strategies with the mechanical velocities of the system.

an isolated load with a resistance of R = 10 was utilised. The simulation was conducted meticulously, allowing for a greater understanding of its characteristics and potential limitations. During this procedure, the conventional control PI was compared to SOSMC, among others, in order to highlight the significance of SOSMC within the control system. The results of this test provide valuable insight into the system's behaviour and efficacy under these particular conditions. The obtained simulation results are depicted in figures 12, 13, and 14.

Figure 12 show Both SOSMC and conventional PI controllers were effective at maintaining the DC bus voltage, demonstrating their usefulness for this particular application. The effective regulation of the DC bus voltage, particularly via the SOSMC, demonstrates the effectiveness of the SOSMC in this context. Nonetheless, we observe that the SOSMC control at 0.2 s does not exceed the reference voltage, which is estimated to be 300 volts. This accomplishment is illustrated by the close correlation between the observed and reference voltages, which demonstrates the robustness and rapid convergence of the SOSMC. In contrast, we observe that the traditional control PI has a significant overrun of up to 340 V. This pattern persists at 7.5 s, where we observe stability in the SOSMC, but there is an-other overshoot in the PI control that reaches 320 V. Despite the fact that both controllers can maintain the DC bus voltage, this comparative analysis emphasis-es SOSMC's more consistent performance.

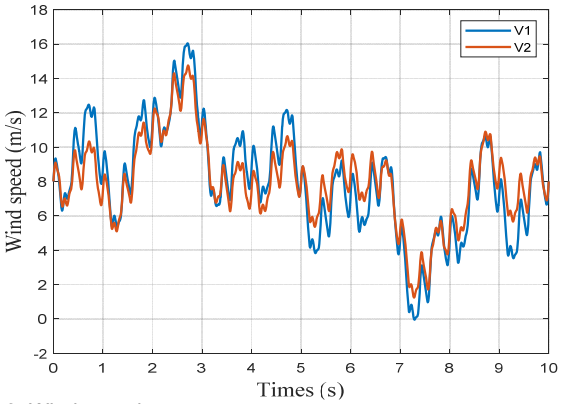

Fig 9: Wind speed.

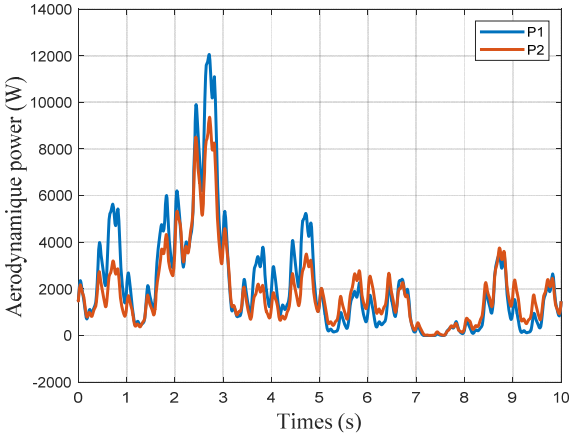

Fig 10: Aerodynamic power (W)

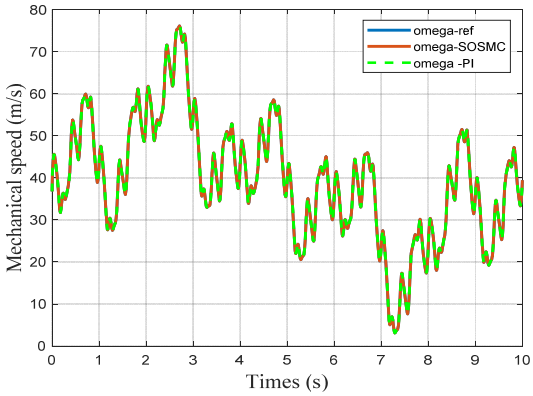

: .

Fig. 11. Mechanical speed.

Figure 13 depicts the stator current, and at 0.2 s and 7.2 s, we observe distinct differences between SOSMC and conventional control PI. SOSMC outperforms conventional PI control with regards to response and monitoring. While SOSMC adheres more closely to the desired parameters, conventional control reveals some excesses at these particular times. When compared to the conventional PI

method, SOSMC provides a more dependable and effective means of control in terms of control stability. In fig. 14, which shows the excitation current, we can see that effective control of the stator current leads to a better excitation current, which shows that the SOSMC does a better job than the traditional control PI. This distinction becomes especially ap-parent at the 0.2s mark, when the SOSMC demonstrates both rapid response and stability. The traditional control PI, on the other hand, exhibits a delayed response with more pronounced excesses. The divergent behaviour of these two control methods at this particular time demonstrates the superior effectiveness of SOSMC in managing the stator current, thereby enhancing the performance of the exit current. The figures also show that both control strategies have to deal with distortions in the output voltage, stator current, and excitation current curves caused by the di-ode rectifier and the high-frequency switching of the chopper connected to the excitation winding.

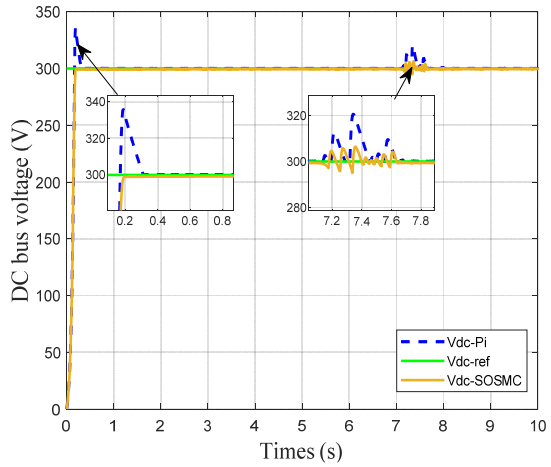

Fig. 12: DC bus voltage (V)

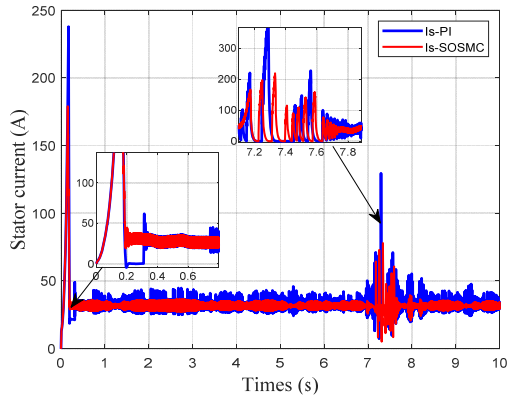

Fig 13: stator current (A)

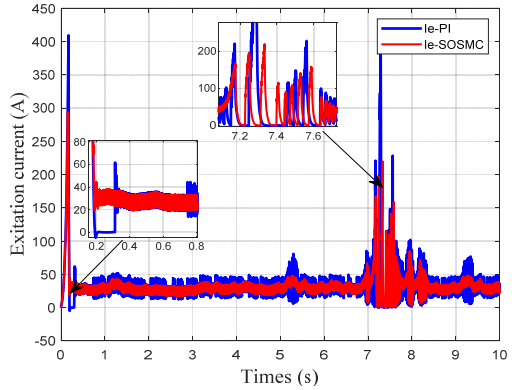

Fig14. Excitation current (A).

In Table 1, we provide a comprehensive comparison of the Proportional-Integral (PI) control and the advanced second-order sliding mode control (SOSMC). This analysis is meticulously formulated, with empirical data extracted from comprehensive and controlled simulation studies serving as its basis. These simulations of real-world operational conditions guarantee the veracity and applicability of the results. The comparison includes several crucial performance parameters, each of which is essential for evaluating the efficacy of a control strategy. In-depth analysis is conducted on parameters such as system stability, control precision, response time, disturbance rejection capability, and tracking accuracy.

Table 1. Comparative results

Performance criteria	PI	SOSMC
Simplicity	Simple	Simple
Dynamic responses	Medium	Fast
Stator currents quality	Acceptable	Good
Control action	Continuous	Continuous
Excitation currents quality	Acceptable	Good
DC bus voltage (V)	Acceptable	Good

Conclusion

In conclusion, this research introduces a novel variable structure control method based on second-order sliding mode (SOSM) control for Wind Energy Conversion Systems (WECS) utilizing two three-phase Hybrid Excitation Synchronous Generators (HESG) connected to a diode bridge rectifier.

Simulation and modeling of the entire system using MATLAB/Simulink demonstrate the success of the proposed conversion method, showcasing its effective-ness for power generation applications. The implementation of SOSM control enhances the performance of traditional control methods, making it a promising solution for the reliable operation of WECS, particularly in the context of renewable energy integration. The results from this study contribute to the advancement of control techniques in wind energy systems and provide valuable insights for re-searchers and industrialists aiming to harness the potential of HESGs for sustain-able energy generation. Future research will concentrate on integrating a wind tur-bine powered by a Hybrid Excitation Synchronous Generator (HESG) with the network. The objective of this project is to design suitable control schemes to ensure the dependability and efficiency of this integration, ensuring that the fluctuating character of wind power does not compromise the grid's stability and performance.

Appendix

Table 2: Parameters of the HESG-WPGS.

System	Parameters
HESG	V = 400 V,f = 50 Hz,p = 6 R_s = 1 Ω,,Rf = 1.35Ω,Ld =Lq= 6 mH,,Lf = 4.4 mH ,M = 4.9mH,phi=0.04Wb
Turbine	R = 1.8 m,Number of blades = 3,G = 1, λ_{opt} = 8.1, $Cpmax$ = 0.48
Load	R=10 Ω

Table 3: Nomenclature and abbreviation

HESG	Hybrid excitation synchronous Generator
WPGS	Wind Power Generator System
SOSMC	Second order sliding mode control
Cp	Coefficient of power
V	Wind speed
Ω_t	mechanical speed of the turbine
Ω_g	generator's mechanical speed
G	The gearbox ratio

Authors
Walid Mohammed KACEMI * *is a PhD student in Hassiba Benbouali University of Chlef,Algeria deparmente of Electrical Engineering mail: w.kacemi@univ-chlef.dz*
Elhadj BOUNADJA *is an Associate Professor at Hassiba Benbouali University of Chlef,Algeria, deparmente of Electrical Engineering mail: e.bounadja@univ-chlef.dz*
Abdelkadir BELHADJ DJILALI *is an Associate Professor at Hassiba Benbouali University of Chlef,Algeria, deparmente of Electrical Engineering mail: a.belhadjdjilali@univ-chlef.dz*
Belkacem SELMA *is a PhD student in Hassiba Benbouali University of Chlef,Algeria deparmente of Electrical Engineering mail: s.belkacem@univ-chlef.dz*

REFERENCES

[1] H. M. Yassin, R. R. Abdel-Wahab, and H. H. Hanafy, "Active and Reactive Power Control for Dual Excited Synchronous Generator in Wind Applications," *IEEE Access*, vol. 10, no. 2169–3536, pp. 29172–29182, Jan. 2022, doi: https://doi.org/10.1109/access.2022.3158621.

[2] G. Gualtieri, "A comprehensive review on wind resource extrapolation models applied in wind energy," *Renewable and Sustainable Energy Reviews*, vol. 102, no. 1364-0321, pp. 215–233, Mar. 2019, doi: https://doi.org/10.1016/j.rser.2018.12.015.

[3] R. R. Abdel-Wahab, H. M. Yassin, and H. H. Hanafy, "Dual Excited Synchronous Generator a Suitable Alternative for Wind Applications," in *2020 IEEE 14th International Conference on Compatibility, Power Electronics and Power Engineering (CPE-POWERENG)*, Jul. 2020. doi: https://doi.org/10.1109/cpe-powereng48600.2020.9161384.

[4] E. Gaughan and B. Fitzgerald, "An assessment of the potential for Co-located offshore wind and wave farms in Ireland," *Energy*, vol. 200, no. 0360-5442, p. 117526, Apr. 2020, doi: https://doi.org/10.1016/j.energy.2020.117526.

[5] C. Jung and D. Schindler, "A review of recent studies on wind resource projections under climate change," *Renewable and Sustainable Energy Reviews*, vol. 165, no. 1364-0321, p. 112596, Sep. 2022, doi: https://doi.org/10.1016/j.rser.2022.112596.

[6] A. Azam, A. Ahmed, H. Wang, Y. Wang, and Z. Zhang, "Knowledge structure and research progress in wind power generation (WPG) from 2005 to 2020 using CiteSpace based scientometric analysis," *Journal of Cleaner Production*, vol. 295, no. 0959-6526, p. 126496, May 2021, doi: https://doi.org/10.1016/j.jclepro.2021.126496.

[7] A. M. S. Yunus, A. Abu-Siada, M. A. S. Masoum, M. F. El-Naggar, and J. X. Jin, "Enhancement of DFIG LVRT Capability During Extreme Short-Wind Gust Events Using SMES Technology," *IEEE Access*, vol. 8, no. 2169–3536, pp. 47264–47271, 2020, doi: https://doi.org/10.1109/access.2020.2978909.

[8] A. Hadi, H. H. Aly, and T. Little, "Harmonics Forecasting of Wind and Solar Hybrid Model Driven by DFIG and PMSG Using ANN and ANFIS," *IEEE Access*, vol. 11, no. 2169–3536, pp. 55413–55424, Jan. 2023, doi: https://doi.org/10.1109/access.2023.3253047.

[9] A. Berrueta, J. Sacristan, J. Lopez, Jose Luis Rodriguez, P. Sanchis, and P. Sanchis, "Inclusion of a Supercapacitor Energy Storage System in DFIG and full-converter PMSG Wind Turbines for Inertia Emulation," *IEEE Transactions on Industry Applications*, vol. 59, no. 1939–9367, pp. 1–9, Jan. 2023, doi: https://doi.org/10.1109/tia.2023.3249145.

[10] F. Liu, K. Wang, and J. C. Li, "Terminal Voltage Oriented Control of Excitation Winding for New AC-Excited Hybrid Excitation Generator," in *International Conference on Electrical Machines and Systems (ICEMS)*, Oct. 2021. doi: https://doi.org/10.23919/icems52562.2021.9634218.

[11] S. Nuzzo, P. Bolognesi, G. Decuzzi, P. Giangrande, and M. Galea, "A Consequent-Pole Hybrid Exciter for Synchronous Generators," *IEEE Transactions on Energy Conversion,* vol. 36, no. 1, pp. 368–379, Mar. 2021, doi: https://doi.org/10.1109/tec.2020.3012198.

[12] Q. Wang, S. Niu, and L. Yang, "Design Optimization of a Novel Scale-Down Hybrid-Excited Dual Permanent Magnet Generator for Direct-Drive Wind Power Application," *IEEE Transactions on Magnetics*, vol. 54, no. 3, pp. 1–4, Mar. 2018, doi: https://doi.org/10.1109/tmag.2017.2758021.

[13] A. Mseddi, S. Le Ballois, H. Aloui, and L. Vido, "Robust control of a wind conversion system based on a hybrid excitation synchronous generator: A comparison between H∞ and CRONE controllers," *Mathematics and Computers in Simulation*, vol. 158, no. 0378-4754, pp. 453–476, Apr. 2019, doi: https://doi.org/10.1016/j.matcom.2018.11.004.

[14] G. Yang, L. Pang, H. Shen, H. Qin, and Chaohui Lisa Zhao, "Influence of excitation current on electromagnetic vibration and noise of rotor magnetic shunt hybrid excitation synchronous motor," *Energy Reports*, vol. 8, no. 2352 4847, pp. 476–485, Nov. 2022, doi: https://doi.org/10.1016/j.egyr.2022.05.227.

[15] S. Hlioui *et al.*, "Hybrid Excited Synchronous Machines," *IEEE Transactions on Magnetics*, vol. 58, no. 2, pp. 1–10, Feb. 2022, doi: https://doi.org/10.1109/tmag.2021.3079228.

[16] Z. Q. Zhu, N. Pothi, P. L. Xu, and Y. Ren, "Uncontrolled Generator Fault Protection of Novel Hybrid-Excited Doubly Salient Synchronous Machines With Field Excitation Current Control," *IEEE Transactions on Industry Applications*, vol. 55, no. 4, pp. 3598–3606, Jul. 2019, doi: https://doi.org/10.1109/tia.2019.2909492.

[17] L. Ye, X. Song, and Z. Chen, "Design and Test of Slender Salient Pole Hybrid Excitation Generator for While Drilling," *Electrical Engineering & Technology* , vol. 17, no. 3, pp. 1741–1749, Jan. 2022, doi: https://doi.org/10.1007/s42835-022-01001-w.

[18] M. Ostroverkhov, V. Chumack, Y. Monakhov, and V. Yu Bazhenov, "Control of a Hybrid Excited Synchronous Generator of an Autonomous Wind Turbine Unit," in *IEEE International Conference on Modern Electrical and Energy Systems (MEES)*, Sep. 2021. doi: https://doi.org/10.1109/mees52427.2021.9598715.

[19] H. Gallas, S. Le Ballois, H. Aloui, and L. Vido, "A hybrid excitation synchronous generator for a 1.5 MW grid-connected wind conversion system," *Electrical Engineering*, vol. 104, no. 6, pp. 4031–4048, Jun. 2022, doi: https://doi.org/10.1007/s00202-022-01585-6.

[20] A. Mseddi, S. Le Ballois, H. Aloui, and L. Vido, "Robust control of a HESG for a wind energy application," *Power Systems,* vol. 168, no. 0378-7796, pp. 250–260, Mar. 2019, doi: https://doi.org/10.1016/j.epsr.2018.12.004.

[21] A. Mseddi, S. Le Ballois, H. Aloui, and L. Vido, "Load mitigation and wind power maximization of a HESG-based wind conversion system," *Renewable and Sustainable Energy,* vol. 12, no. 5, pp. 053305–053305, Sep. 2020, doi: https://doi.org/10.1063/5.0009642.

[22] H. Gallas, "Contribution à la Commande d'un Générateur de type Synchrone à Double Excitation dans le cas d'une Application Éolienne et Comparaison avec d'autres Architectures," 2021. Accessed: Jul. 12, 2023. [Online]. Available: https://hal.science/tel-03433652

[23] N. Patin, L. Vido, E. Monmasson, J.-P. . Louis, M. Gabsi, and M. Lecrivain, "Control of a Hybrid Excitation Synchronous Generator for Aircraft Applications," *IEEE Transactions on Industrial Electronics*, vol. 55, no. 10, pp. 3772–3783, Oct. 2008, doi: https://doi.org/10.1109/tie.2008.924030.

[24] C. Jiang *et al.*, "Hybrid excitation control strategy of the synchronous condenser using differential geometry principle assisted with a PI controller," in *2019 14th IEEE Conference on Industrial Electronics and Applications (ICIEA)*, Jun. 2019. doi: https://doi.org/10.1109/iciea.2019.8833793.

[25] W. M. KACEMI, E. BOUNADJA, and A. B. DJILALI, "DC Voltage Output Control of a Hybrid Synchronous Generator-based Wind Turbine," *International Journal of Advanced Natural Sciences and Engineering Researches*, vol. 7, no. 4, pp. 169–174, May 2023, doi: https://doi.org/10.59287/ijanser.645.

[26] A. Mseddi, "Modélisation et commande d'un générateur éolien à double excitation isolé en vue de l'amélioration de son rendement et de la diminution de la fatigue mécanique," 2019. Accessed: Jul. 12, 2023. [Online]. Available: https://theses.hal.science/tel-02888660

[27] B. J. Parvat and S. D. Ratnaparkhi, "A Second Order Sliding Mode Controller Applications in Industrial Process," *International Journal of Engineering Trends and Technology*, vol. 19, no. 4, pp. 217–222, Jan. 2015, doi: https://doi.org/10.14445/22315381/ijett-v19p238.

[28] Ferhat Bodur and O. Kaplan, "Second-Order Sliding Mode Control Algorithms in DC/DC Buck Converter," in *10th International Conference on Smart Grid (icSmartGrid)*, Jun. 2022. doi: https://doi.org/10.1109/icsmartgrid55722.2022.9848696.

[29] D. Castellanos-Cárdenas, F. Castrillón, R. E. Vásquez, N. L. Posada, and O. Camacho, "A new Sliding Mode Control tuning approach for second-order inverse-response plus variable dead time processes," *Journal of Process Control,* vol. 115, pp. 77–88, Jul. 2022, doi: https://doi.org/10.1016/j.jprocont.2022.05.001.

[30] M. Vásquez, J. Yanascual, M. Herrera, A. Prado, and O. Camacho, "A hybrid sliding mode control based on a nonlinear PID surface for nonlinear chemical processes," *Engineering Science and Technology, an International Journal*, vol. 40, pp. 101361–101361, Apr. 2023, doi: https://doi.org/10.1016/j.jestch.2023.101361.